Optimal Building Thermal Load Scheduling for Simultaneous Participation in Energy and Frequency Regulation Markets †

Jie Cai

School of Aerospace and Mechanical Engineering, University of Oklahoma, Norman, OK 73072, USA;
jcai@ou.edu

† This paper is an extended version of our paper published in 2020 American Control Conference,
Denver, CO, USA, 1–3 July 2020; pp. 4219–4224.

Abstract: This paper presents an optimal scheduling solution for building thermal loads that simultaneously participate in the wholesale energy and frequency regulation markets. The solution combines (1) a lower-level regulation capacity reset strategy that identifies the available regulation capacity for each hour, and (2) an upper-level zone temperature scheduling algorithm to find the optimal load trajectory with a minimum net electricity cost. In the supervisory scheduling strategy, piece-wise linear approximations of representative air-conditioning equipment behaviors, derived from an offline analysis of the capacity reset mechanism, are used to predict the cooling power and regulation capacity; and a mixed-integer convex program is formulated and solved to determine the optimal control actions. In order to evaluate the performance of the developed control solution, two baseline strategies are considered, one with a conventional night setup/back control and the other utilizing an optimization procedure for minimizing the energy cost only. Five-day simulation tests were carried out for the various control strategies. Compared to the baseline night setup/back strategy, the energy-priority controller led to a 26% lower regulation credit and consequentially caused a net cost increase of 2%; the proposed bi-market control solution was able to increase the regulation credit by 118% and reduce the net electricity cost by 14%.

Keywords: demand-side management; frequency regulation; demand response; load scheduling; model-predictive control

1. Introduction

One essential task for power system operation is to maintain the real-time supply and demand balance, in order to keep the system frequency stable. However, the ever-increasing penetration of renewable energy resources on the electric grid contributes to uncertainties and intermittencies of power generation, which poses challenges to grid reliability and stability. Unexpected generator failures also cause frequency stability issues. On 9 August 2019, Britain experienced the most severe blackout in more than a decade, which was caused by the grid frequency dropping below the safety limits following two generator outages [1]. To alleviate the frequency stability concerns and to improve grid resiliency against the risk of generator failures, the power markets have seen dramatic increase in the procurement of frequency regulation service in recent years [2].

Heating, ventilation and air conditioning (HVAC) systems in buildings are responsible for 24% of the total electricity usage in the U.S. [3] and are excellent candidates for power frequency regulation due to the inherent thermal inertia. Various types of HVAC equipment have been investigated for regulation service, such as variable-speed supply fans [4,5], electrical space heaters [6], chilled-water pumps [7], residential heat pumps [8], water heaters [9], commercial-scale chillers [10] and packaged air-conditioning equipment [11]. In addition to frequency regulation support for the bulk power grid, HVAC equipment was also successfully used for frequency support of microgrids [12,13] and for load following in mitigating renewable power fluctuations [14]. The published results have demonstrated

a variety of advantages of using HVAC equipment for frequency regulation compared to other resources on the market:

- *Ramping rate*: HVAC equipment can respond to frequency deviations much faster than traditional generator-side control [15];
- *Efficiency loss*: although prior studies reported noticeable round-trip efficiency losses during frequency regulation control of variable-speed fans [16], recent laboratory tests with controlled environments have shown negligible efficiency loss or even sensible efficiency gains when appropriate regulation control strategies are adopted [11]; in [17], it was also proved through a rigorous analysis that regulation control of HVAC equipment does not cause efficiency losses;
- *Regulation performance*: incorporating regulation strategies in OEM controllers could result in PJM (Pennsylvania-New Jersey-Maryland Interconnection, a regional transmission organization serving the northeast of U.S.) regulation performance scores of up to 0.98; even with an add-on (after-market) regulation control solution, regulation scores of above 0.9 were obtained consistently [11];
- *Procurement cost*: HVAC equipment is installed in almost every building; thus, the procurement cost is relatively lower compared to other regulation resources, such as batteries.

There are also limiting factors for buildings' participation in the frequency regulation market. Most regulation markets in the U.S. have minimum size requirements for the bidders [18], e.g., the PJM regulation market has a minimum capacity requirement of 0.1 MW [19]. The relatively small power capacity in a single building, especially for the residential and light commercial sectors, represents a major barrier for buildings' contribution to frequency regulation. However, a number of buildings can be aggregated or coordinated to offer adequate sizes of regulation service; attempts were made to develop aggregation strategies for multi-building frequency regulation control, e.g., [20–23] to eliminate the size issue of frequency regulation in a single building.

Time-varying availability of the HVAC regulation capacity is regarded as another disadvantage. HVAC equipment is primarily used to deliver indoor comfort and the variable cooling load, to a large extent, dictates the available regulation service that can be provided by HVAC equipment. For symmetric markets such as PJM, the HVAC regulation capacity is lower at excessively high or low load conditions. When a variable-capacity AC unit is running close to its full load, there is not much room for the unit power to ramp up, leading to limited regulation capacities. However, regulation control can be combined with load shifting techniques, e.g., through zone temperature setpoint reset, to adapt the availability of the HVAC regulation capacity in response to grid needs. This control problem is often formulated as a multi-market scheduling program in which the net cost (energy cost minus the frequency regulation credit) is minimized. Maasoumy et al. [24] proposed a model-predictive control strategy to reduce a building's net electricity cost when participating in wholesale energy and frequency regulation markets. A min-max problem was formulated to ensure robust control performance under all possible realizations of the random regulation signal. Vrettos et al. [25,26] developed and experimentally demonstrated a hierarchical frequency regulation control solution for supply air fans in commercial buildings. The solution uses a supervisory reserve scheduler to identify the regulation reserve capacity for the next day, a room controller to find the most efficient supply air flow setpoints and a local regulation signal tracking controller. The reserve scheduler adopts a similar robust formulation as in [24] by explicitly considering the randomness in the regulation signal. The approaches adopted by [24–26] all relied on supply air fans to provide frequency regulation; fan control is straightforward but its power capacity is much smaller compared to that of compressors in a HVAC system. Blum et al. [27] developed a multi-market optimization strategy for multi-zone commercial buildings considering control optimization of both the fan and chiller. In addition to frequency regulation and wholesale energy markets, reserve service was also considered. In another paper by Blum et al. [28], the trade-off between the energy cost and regulation reward was investigated from a different point of view, through evaluating the opportunity cost associated with HVAC frequency regulation; the oppor-

tunity cost was calculated as the increased energy cost during regulation control, which would have been avoided when using energy-optimal control strategies. Pavlak et al. [29] recognized the difficulties of HVAC dual-market (energy plus frequency regulation) control due to the system nonlinear behaviors, and proposed a predictive scheduling solution that incorporates a zone temperature perturbation approach to estimate the regulation reserve for each hour. The optimization problem in their work required 1–6 h of machine time to solve on a twelve-core workstation, which poses challenges for practical implementation of the proposed approach.

It is evident that an efficient dual-market control strategy for building thermal loads is lacking, but is of great importance to accommodate the growing demand for frequency regulation support of the electric grid. In this paper, we present an efficient and practical load scheduling strategy to support buildings' simultaneous participation in the wholesale energy and frequency regulation markets. The strategy adopts a bi-level control structure where (1) a lower-level regulation capacity reset strategy is implemented every hour to identify the control settings that provide the maximum regulation capacity and (2) a supervisory load scheduling algorithm is called, in a receding horizon manner, to seek the optimal zone temperature trajectory for minimizing the net electricity cost. The original problem is highly nonlinear and involves mode switches due to minimum compressor/fan speed constraints. To improve the numerical feasibility, an offline analysis was performed for the lower-level capacity reset strategy covering all possible operating conditions. Using the offline optimization results, piece-wise linear approximations of the lower-level control behaviors were obtained and used in the supervisory scheduling algorithm. With the lower-level control approximations, the overall problem can be converted to a mixed-integer convex program which can be solved very efficiently. In the simulation tests, each 24-h scheduling problem only took less than 0.2 s to solve on a regular laptop with an i5 processor and 8 GB ram. The developed control solution, derived based on a comprehensive HVAC performance model, explicitly accounts for actual operation characteristics, such as compressor/fan speed constraints and system part-load efficiencies. All these features make the proposed solution practical to implement with performance close to optimal.

The paper is structured as follows. Section 2 summarizes prior laboratory test results of the lower-level regulation capacity reset strategy and describes the case study. Section 3 introduces the control and/or simulation models for the various components involved in the case study. The proposed control strategy as well as two baseline strategies are elaborated in Section 4 and the key simulation results are presented and discussed in Section 5. Concluding remarks are given in Section 6.

2. Case Study Description and Prior Results

2.1. Case Study

This study considers a small office building served by a 5-ton (17.5 kW) variable-speed air-conditioning (AC) system. The system employs a direct-expansion vapor-compression circuit with variable air volume comfort delivery. The building has four thermal zones with a total floor area of approximately 400 m^2 and is used as graduate student offices. A data-driven model was established to characterize the envelope dynamics using field data and the model was validated with data collected in different seasons [30]. The AC system employs variable-speed drives for the compressor, supply fan and condenser fan. The onboard controller uses the following built-in logics for speed control: the supply fan speed is varied to maintain the zone air temperature (ZAT) setpoint and the compressor speed is modulated to achieve a desired supply air temperature (SAT) setpoint. The condenser fan speed is set in sync with the compressor speed. Although component speeds cannot be controlled externally, the ZAT and SAT setpoints can be adjusted by any BACnet-compatible control system as a means to indirectly control the component speeds.

2.2. Prior Results

The author previously developed a frequency regulation control strategy for the considered AC system [31]. The strategy assumes a hierarchical control scheme: a regulation capacity reset algorithm is executed prior to each bidding interval, e.g., one hour, to identify the available regulation capacity for the upcoming bidding period; a fast regulation power tracking controller adjusts the SAT setpoint in real-time (every second) to modulate the compressor power in order to follow the regulation signal. The hourly capacity reset algorithm takes the current cooling load, estimated with a moving average filter, and implements a pseudo-optimization routine to determine an appropriate regulation reference power and the upper and lower limits, which together dictate the regulation capacity. The optimization routine aims to maximize the regulation capacity while satisfying relevant operation constraints, such as the load requirements and compressor/fan speed limits. The hourly capacity reset strategy is summarized in Section 4.1 of the present paper. The real-time regulation tracking control is implemented in a feedback scheme for dynamic reset of the SAT setpoint as a means to indirectly control the compressor power. The supply fan speed is varied by the original thermostat controller to maintain the ZAT setpoint and indoor comfort.

Figure 1 shows example laboratory test results of the previously developed frequency regulation control strategy [31]. The test was conducted in twin psychrometric chambers. Since the chambers have significantly different dynamics compared to an actual building, a load-based testing approach was implemented, in which the indoor chamber temperature was varied according to a lumped capacitance load model to reproduce realistic responses of indoor thermal conditions. In the load model, a representative thermal capacitance value was identified based on thermostat data collected in a dozen of houses. The 3rd subplot in Figure 1 depicts the variation of the ZAT during the test. The results proved that HVAC frequency regulation has negligible impact on indoor temperature control, with temperature fluctuations smaller than 0.5 °C around the setpoint (23.5 °C). The test mirrored a 6-h morning scenario with a monotonically increasing cooling load, as depicted in the 4th subplot. The 1st subplot shows variations of the regulation signal (actual PJM historical signal), actual unit power response and the hourly regulation band, determined by the regulation capacity reset strategy. The 2nd subplot shows the SAT setpoint generated by the regulation controller as well as the actual SAT value. It can be seen that with the developed regulation control strategy, the AC unit power was able to closely follow the regulation signal and the calculated hourly PJM performance scores were almost always above 0.9. Using PJM historical regulation and wholesale energy prices, we have demonstrated significant economic benefits for building owners if HVAC systems can be used to provide frequency regulation service. The regulation credit could offset up to 45% of the hourly AC electricity cost at the most favorable conditions.

However, previous test results, obtained under a conventional night setup control for the ZAT, also revealed that the regulation availability of a HVAC system varies significantly with load and other operating conditions. As can be seen in the 1st subplot of Figure 1, there is limited regulation capacity during high- or low-load hours, because the compressor speed can only be modulated in a limited range, e.g., 39% to 100% for the considered AC unit. The extreme load requirements could result in a baseline compressor speed close to the upper or lower limit, leading to reduced speed modulation margins. The variable regulation capacity limits the total regulation service (as well as regulation credits) from HVAC equipment using the conventional night setup/back control. A previous simulation study [31] showed that the daily utility savings, associated with regulation credits, drops to 26% from the maximum hourly savings of 45%.
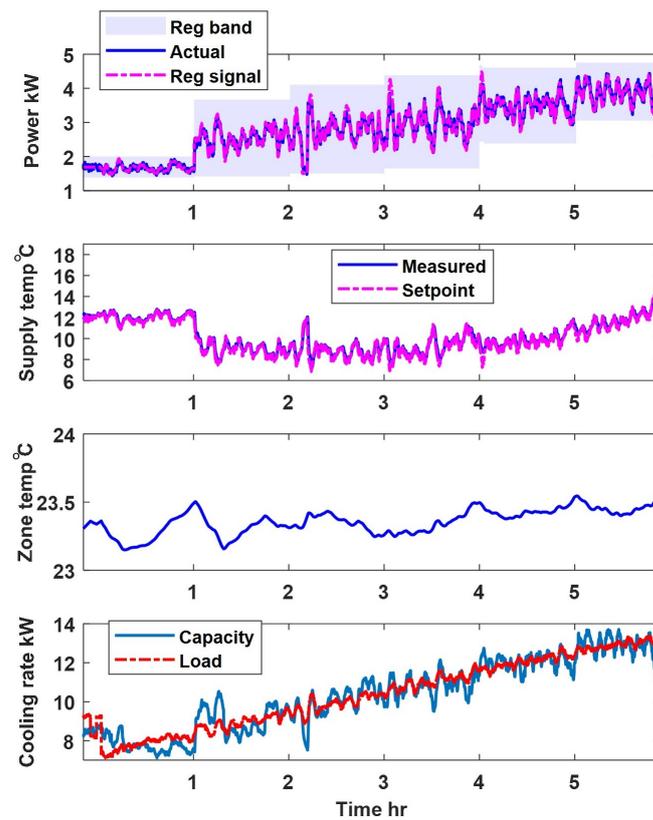
Figure 1. Laboratory test results of frequency regulation for a 5-ton variable-speed rooftop unit.

2.3. New Contributions

A building load profile can be optimally shaped through ZAT scheduling to maximize the daily regulation capacity or minimize the net electricity cost. The present work expands beyond the previously developed frequency regulation strategy by including a predictive load scheduler to improve a building's frequency regulation availability. The control diagram is given in Figure 2 where the shaded box indicates the strategies proposed in the present work. The fast regulation power tracking control strategy has been validated through extensive laboratory tests and is not considered in this paper.
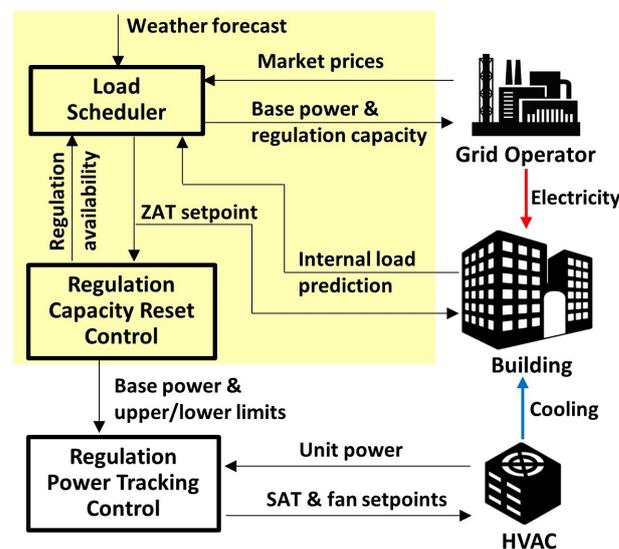

Figure 2. Control diagram of proposed strategy.

3. Models

This section introduces the various component models used in the simulation tests and control strategies. It should be noted that the same building envelope model, derived and validated with field data, is used for control synthesis and simulation tests. For power consumption and regulation behaviors of the AC equipment, different control and simulation models are utilized.

3.1. Building Envelope

A thermal network model is used to emulate the indoor temperature responses for given cooling rates delivered by the AC system. Assuming constant convective and radiative heat transfer coefficients between the indoor/outdoor air body and wall interior/exterior surfaces, a linear time invariant (LTI) discrete-time state-space model can be established:

$$\mathbf{x}[i+1] = \mathbf{A}\mathbf{x}[i] + \mathbf{B}_w \mathbf{w}[i] + \mathbf{B}_u q[i] \tag{1}$$

$$y[i] = \mathbf{C}\mathbf{x}[i] = x_z[i] \tag{2}$$

where $\mathbf{x}$ is the state vector consisting of all nodal temperatures in a building thermal network; x_z is the state variable corresponding to the zone air temperature; $\mathbf{w}$ is comprised of non-controllable disturbance inputs including weather conditions and internal heat gains from occupants and electrical appliances; q is the sensible cooling effect generated by the AC system, which is the only controllable input; y is the model output. The matrices $\mathbf{A}$, $\mathbf{B}_w$, $\mathbf{B}_u$ and $\mathbf{C}$ are constructed based on values of the thermal resistances and capacitances involved in the thermal network and are time invariant.

An envelope model for the case study building was identified, with the resistance and capacitance values estimated using two weeks of operation data. The thermal network of the model consists of two 3-resistance-2-capacitance wall branches, one for the external wall representing the main indoor-outdoor thermal coupling and the other branch for a concrete floor which contributes the majority of building thermal mass. The model also includes a 1-resistance window branch capturing fast thermal interactions with the ambient. The model has been validated with data collected across different seasons. Modeling details and training/validation results can be found in [30]. The building moisture dynamics are not considered, since the case study simulations used actual field data that involved relatively dry weather. For cases with non-negligible latent loads, a moisture network modeling approach, which preserves the LTI feature in the resultant model, can be used to capture the indoor humidity dynamics [32] to which the proposed control solution is still applicable.

3.2. AC System

A quasi-steady-state model for variable-speed direct-expansion AC equipment is utilized to predict the cooling capacity (q) and unit power consumption (p) for given outdoor temperature (T_o), return air dry-bulb temperature (T_i), compressor speed (s) and supply air flow rate (m_a):

$$[q, p] = \mathrm{AC}(T_i, T_o, m_a, s). \tag{3}$$

The model is a variant of the ASHRAE Toolkit model, which calculates the total cooling capacity and energy input ratio using polynomial-type correlations with respect to ambient temperature, evaporator inlet wet-bulb temperature and airflow rate. The modified model applies an additional correlation factor that is in a quadratic form of the compressor speed, to capture its impact on the system efficiency and cooling output. The bypass factor method is employed to estimate the sensible heat ratio (SHR). For dry-coil operation, the use of the evaporator wet-bulb temperature would result in an underestimation of the total capacity and a SHR greater than unity. Therefore, an iterative process is implemented for dry-coil scenarios to find a fictitious wet-bulb temperature that generates a SHR equal to unity, and the corresponding capacity and power are used as final model outputs. The original AC model requires both the dry- and wet-bulb temperatures of the air entering the evaporator

coil as inputs. However, due to the dry weather and small latent load involved in the case study, a fixed relative humidity of 30% is used in the AC model and that is why the wet-bulb temperature input is dropped in Equation (3). The AC model was trained using manufacturer performance data and the details can be found in [33].

3.3. Wholesale Energy and Frequency Regulation Markets

The PJM hour-ahead energy and frequency regulation markets are considered in this study to demonstrate the efficacy of the proposed control solution. The PJM market requires regulation resources to provide a bid of reference power, regulation capacity, and price prior to each hour of clearing interval. If the offer is accepted, a regulation credit is issued to the resource after the hour of service and the credit depends on the capacity, performance of the provided service and the clearing price [34]. For demand-side resources, the net energy cost for each hour is

$$c_n = e \cdot r_e - p_c \cdot r_{fr}. \tag{4}$$

where e is the hourly electricity use (kWh), r_e is the wholesale energy price ($/kWh), p_c is the regulation capacity (kW), and r_{fr} is the combined frequency regulation price ($/kW). The PJM regulation market has two types of credits, associated with the capacity and performance, respectively, that are calculated as

$$cr_c = p_c \cdot \rho \cdot r_{fr,c}$$
$$cr_p = p_c \cdot \rho \cdot r_{fr,p} \cdot \alpha$$

where $r_{fr,c}$ (cr_c) and $r_{fr,p}$ (cr_p) are the capacity and performance clearing prices (credits), respectively, ρ is the performance score, and α is the mileage ratio which is defined as ratio of the actual regulation signal mileage to the average PJM RegA mileage. Thus, for RegA (traditional) service, the mileage ratio is close to unity while the RegD (dynamic) service involves a much higher mileage ratio (α of RegD is close three based on historical PJM market data). The combined regulation price r_{fr} incorporates both credits as

$$r_{fr} = \rho \cdot (r_{fr,c} + r_{fr,p} \cdot \alpha).$$

Figure 3 shows the average diurnal variations of the wholesale energy (locational marginal price, LMP) and combined regulation prices over the year of 2018, based on PJM historical data. The plotted regulation price was calculated for RegD ($\alpha = 3$) based on a performance score of 0.95 (averaged regulation performance from previous laboratory tests [11]).
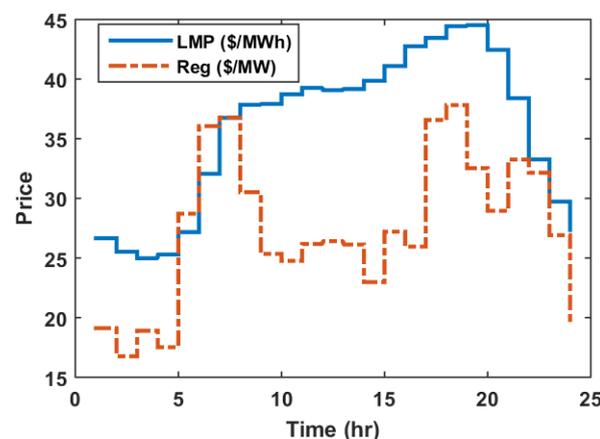

Figure 3. PJM annual average prices in 2018.

4. Bi-Market Control Strategy

As shown in Figure 2, the proposed strategy consists of a regulation capacity reset controller (lower-level) that maximizes the hourly regulation flexibility and a supervisory scheduler (upper-level) to find the optimal ZAT trajectory with minimum net operation costs. In practical implementations, this bi-level control strategy is executed prior to each bidding interval, e.g., every hour for PJM markets; the obtained control parameters, such as the ZAT setpoint and regulation capacity, are fed to the fast regulation power tracking controller (not considered in the present study) which adjusts the SAT setpoint every a few seconds to follow the dynamic regulation signal.

4.1. Regulation Capacity Reset

The regulation capacity reset strategy takes the baseline AC load (determined by the ZAT setpoint generated by the supervisory scheduler) and other operating conditions and outputs the regulation capacity at each hour of operation, by solving the optimization problem

$$\max_{\{s, m_a\}} \left(\min(\bar{s} - s, s - \underline{s}) \right) \tag{5}$$

subject to

$$q = \mathrm{AC}_q(T_i, T_o, m_a, s) \tag{6}$$

$$\underline{m_a} \leq m_a \leq \overline{m_a} \tag{7}$$

$$\underline{s} \leq s \leq \bar{s} \tag{8}$$

$$\underline{T}_{sa} \leq \mathrm{AC}_{SAT}(T_i, T_o, m_a, \bar{s}) \tag{9}$$

$$\overline{T}_{sa} \geq \mathrm{AC}_{SAT}(T_i, T_o, m_a, \underline{s}) \tag{10}$$

where the underscored and overlined symbols represent the lower and upper limits of the corresponding variables. The problem aims to maximize the compressor speed modulation margin $\Delta s = \min(\bar{s} - s, s - \underline{s})$ (equivalent to maximizing the regulation capacity). The function subscript indicates the specific sub-function that outputs the corresponding variable, e.g., AC_q represents the sub-function of "AC" that calculates the cooling capacity q. The first constraint ensures that the average cooling rate delivered by the AC unit matches the load within the bidding interval. The second and third constraints make sure the baseline airflow and compressor speed fall within the respective feasible regions. The airflow rate tends to have a slow variation due to the small PI gains used by the thermostat controller. The compressor speed, which is the actuating variable to maintain the desired SAT setpoint, can change at a more aggressive rate because of the fast SAT dynamics; this makes tracking of a fast regulation signal possible. The last two constraints enforce the SAT setpoint upper and lower limits (i.e., $\overline{T}_{sa}$ and $\underline{T}_{sa}$) during regulation control. These SAT constraints are necessary for the considered AC unit, because direct compressor speed control is not available and compressor power modulation is achieved by adjusting the SAT setpoint; the unit can only accept a SAT setpoint from 45 °F (7.2 °C) to 65 °F (18.3 °C). For AC systems whose compressor speed can be directly controlled, the last two constraints can be dropped.

For variable-capacity AC systems, both the compressor and fan speeds are controllable. Therefore, to meet a given cooling load, there is one degree of freedom for control optimization and the regulation capacity reset controller aims to identify the optimal compressor and fan speed combination to achieve the maximum regulation capacity. Figure 4, a contour plot of the AC cooling output with variable compressor speed and airflow rate, illustrates the optimization process. The shaded areas indicate the infeasible regions where the SAT goes outside the allowed range. For the considered AC unit, the compressor speed is allowed to vary between40% and 100% of its nominal speed. Thus, an ideal base compressor speed setting is 70%, for which the speed is free to ramp up or down within its maximum margin of 30%. However, this speed setting may be sub-optimal or

even infeasible due to load and SAT constraints. In Figure 4, the optimal operation points for cooling loads of 11 kW and 8 kW are highlighted. For the 11 kW load case, optimal operation is achieved at a base compressor speed of 70% and airflow fraction of 72%, and no other constraints are active in the full compressor speed modulation range. For the scenario with a 8 kW load, the 70% compressor speed is not even in the feasible region due to the low load. The SAT lower limit of 45 °F (7.2 °C) further limits the compressor speed modulation margin; the optimal regulation operation occurs at the base compressor speed of 58% and airflow fraction of 42% with a compressor modulation margin of 18%. The regulation capacity reset strategy essentially glides on the constant-load curve and seeks the optimal point that leads to the maximum compressor speed modulation margin.
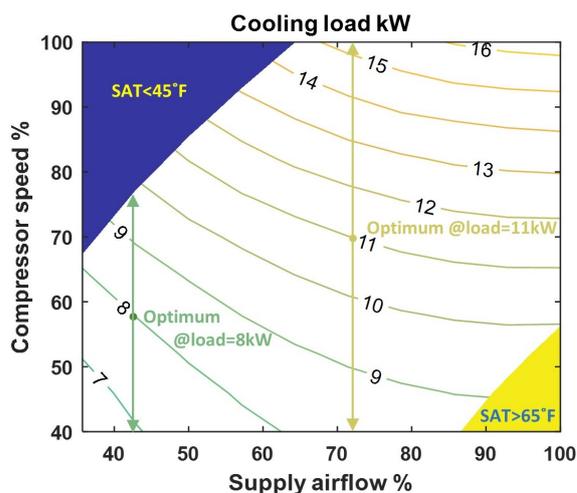

Figure 4. Illustration of the capacity reset strategy.

Once the optimal control settings are determined, the regulation power upper and lower limits can be determined as

$$\overline{p} = \mathrm{AC}_p(T_i, T_o, m_a, s + \Delta s)$$
$$\underline{p} = \mathrm{AC}_p(T_i, T_o, m_a, s - \Delta s).$$

The regulation capacity is $p_c = (\overline{p} - \underline{p})/2$ and the reference AC power is $p = \mathrm{AC}_p(T_i, T_o, m_a, s)$, which together dictate the regulation flexibility. This is a reasonable approach to estimate the flexibility because the compressor power has a close-to-linear relationship with its speed. It should be noted that the regulation flexibility is dependent on the hourly load, which is determined by the supervisory scheduler.

4.2. Supervisory Scheduler

The supervisory scheduler seeks the optimal ZAT setpoint trajectory and the corresponding load schedule in a look-ahead horizon. The scheduler considers a bi-market control problem and aims to minimize the net cost within the control horizon:

$$\min \sum_{i \in \mathcal{I}_k} \left\{ e[i] \cdot r_e[i] \cdot - p_c[i] \cdot r_{fr}[i] \right\} \tag{11}$$

subject to

$$\mathbf{x}[i+1] = \mathbf{A}\mathbf{x}[i] + \mathbf{B}_w \mathbf{w}[i] + \mathbf{B}_u q[i], \qquad \forall i \in \mathcal{I}_k \tag{12}$$
$$T_{lb}[i+1] \leq \mathbf{C}\mathbf{x}[i+1] \leq T_{ub}[i+1], \qquad \forall i \in \mathcal{I}_k \tag{13}$$
$$[p[i], p_c[i]] = \mathcal{CR}(T_i, T_o[i], q[i]), \qquad \forall i \in \mathcal{I}_k \tag{14}$$

where $\mathcal{I}_k = \{k, ..., k + N_p - 1\}$ is the set of time indices for the look-ahead time horizon, k indicates the current time step, N_p is the length of the prediction horizon, and T_{lb} and T_{ub} are the lower and upper limits of zone temperature to ensure indoor comfort. The comfort limits are time indexed because they vary from one time step to another depending on the occupancy status. The last constraint is associated with the capacity reset controller described in Section 4.1, where $\mathcal{CR}$ is the capacity reset operator. p is the baseline cooling power, Δt is the time step, and $e[i] = p[i] \cdot \Delta t$ is the integrated electricity use for time step i. The capacity reset operator is highly nonlinear and non-convex due to the nonlinearity in the AC model, which makes the scheduling problem difficult to solve directly. To improve the computational feasibility, a control-friendly surrogate model is needed to approximate the behaviors of the capacity reset controller.

At each time step, the maximum cooling capacity that the AC system can provide is $\bar{q} = \text{AC}_q(T_i, T_o, \overline{m}_a, \bar{s})$ (the time indices are dropped for ease of notation). An auxiliary variable, load ratio $\mathbb{q}$, is introduced to represent the ratio of the instantaneous cooling demand to the maximum capacity, i.e., $\mathbb{q} = q/\bar{q}$. The capacity reset operator requires the indoor temperature (or mixed air temperature at the evaporator inlet for cases with non-zero ventilation rates) to determine the regulation flexibility. This represents a major coupling between the capacity reset controller and the building envelope dynamics. For ease of control synthesis, this coupling effect can be eliminated by fixing the indoor temperature T_i to its upper limit T_{ub} of occupied hours. This is an acceptable simplification since optimal control actions tend to maintain the indoor temperature at the upper bound during hours with non-zero cooling loads. With this simplification, $\bar{q}$ is a function of T_o only. The cooling demand can be represented as $q = \mathbb{q} \cdot \bar{q}$. The AC power ratio is defined in a similar way as $\mathbb{p} = p/\bar{p}$ where $\bar{p}$ is the total AC power when running at full speeds, i.e., $\bar{p} = \text{AC}_p(T_i, T_o, \overline{m}_a, \bar{s})$. The regulation capacity ratio is defined as $\mathbb{p}_c = p_c/\bar{p}$. Then the regulation capacity reset operator can be re-written as

$$[\mathbb{p}, \mathbb{p}_c] = \mathcal{CR}(T_o, \mathbb{q}).$$

The regulation capacity reset control problem formulated in (5)–(10) was solved offline for different ambient temperatures and load ratios. The obtained optimal results for AC power ratio and regulation capacity ratio are depicted in Figures 5 and 6, respectively. The *x*-axis gives the load ratio $\mathbb{q}$. The *y*-axis corresponds to the power ratio $\mathbb{p}$ in Figure 5 and the regulation capacity ratio $\mathbb{p}_c$ in Figure 6.
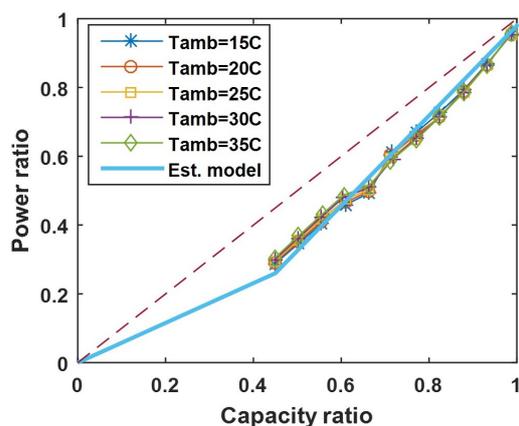

Figure 5. Variation of power ratio with capacity ratio.

Figure 5 shows that the minimum load ratio occurs at the minimum compressor speed ($\underline{s}$, 40% of nominal speed) and airflow rate ($\underline{m}_a$, 35% of nominal airflow), and is close to 0.45. It can be observed that the ambient temperature has a negligible impact on the functional relationship between $\mathbb{p}$ and $\mathbb{q}$. The dashed line represents a constant-efficiency scenario where the cooling coefficient of performance (COP) is equal to the full load COP. It can

be seen that during continuous AC operation (load ratio greater than 0.45), the system efficiency is always higher (lower power consumption) than that of the full load, mainly due to reduced pressure lifts across the compressor. Furthermore, the power ratio variation with respect to the load ratio is close to linear. For load ratios lower than 0.45, the AC unit starts cycling on and off to meet the demand and it is assumed that the efficiency remains the same as that at the minimum cooling output. A 2-segment piece-wise linear fit was obtained, which is shown as the solid lines in Figure 5, and can be represented in a convex form:

$$\mathbb{p} = \max(0.58\mathbb{q}, 1.31\mathbb{q} - 0.33). \tag{15}$$

Figure 6 depicts the optimal regulation capacity for different load and ambient conditions. When the load drops below the minimum cooling output, the unit starts cycling and no regulation service can be provided, because of the symmetric regulation requirement of the PJM market. When the load increases beyond the minimum cooling rate, the regulation capacity becomes nonzero and starts to increase as the load gets higher. When the load reaches a threshold (load ratio of 0.77), the available regulation capacity drops as the load continues to increase (compressor speed approaching the upper limit). The variation of the regulation capacity does not change much as the ambient temperature varies; therefore, its dependence on T_o can be safely neglected. Three linear fits were obtained for the respective load segments, represented by the solid lines in Figure 6. The overall regulation capacity variation is not concave, due to the existence of the segment for cyclic operation ($\mathbb{q} \in [0, 0.45]$); this makes the overall scheduling problem non-convex. To improve the computational feasibility, the piece-wise linearity is leveraged to reformulate the problem into a mixed-integer program (MIP), the solution of which is more computationally tractable (still NP-hard).
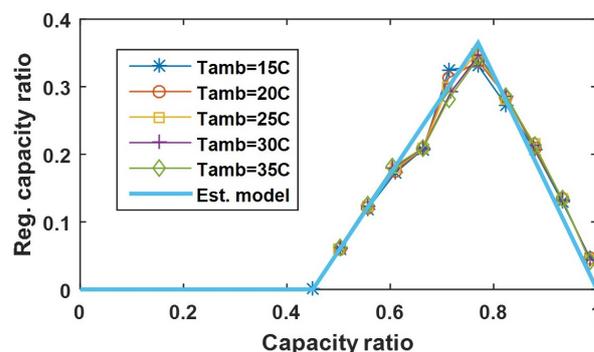

Figure 6. Variation of regulation capacity ratio with capacity ratio.

One MIP formulation for a general 3-segment piece-wise linear function, as shown in Figure 7, is

$$\mathbb{q} = a_0\lambda_0 + a_1\lambda_1 + a_2\lambda_2 + a_3\lambda_3 \tag{16}$$

$$\mathbb{p}_c = b_0\lambda_0 + b_1\lambda_1 + b_2\lambda_2 + b_3\lambda_3 \tag{17}$$

$$1 = \lambda_0 + \lambda_1 + \lambda_2 + \lambda_3 \tag{18}$$

$$1 = y_1 + y_2 + y_3 \tag{19}$$

$$\lambda_0 \leq y_1 \tag{20}$$

$$\lambda_1 \leq y_1 + y_2 \tag{21}$$

$$\lambda_2 \leq y_2 + y_3 \tag{22}$$

$$\lambda_3 \leq y_3 \tag{23}$$

$$0 \leq \lambda_j, \qquad \forall j \in \{0, 1, 2, 3\} \tag{24}$$

$$y_j \in \mathcal{B} = \{0, 1\}, \quad \forall j \in \{1, 2, 3\} \tag{25}$$

where a_0 to a_3 represent the endpoints of the 3 segments, and b_0 to b_3 are the functional values at the four endpoints. The independent variable $\mathbb{q}$ is formulated as a convex combination of the four endpoints with λ_0 to λ_3 being the coefficients. It may be noted that there are infinite number of coefficient combinations to represent a given point. To obtain a unique representation, binary variables y are introduced. Equation (19) ensures only one y is nonzero, say y_j. Equations (20)–(23) guarantee that the point $\mathbb{q}$ falls on the jth segment and only the two coefficients of the corresponding segment endpoints are nonzero, resulting in a unique representation for each $\mathbb{q}$ value. Define $\mathbf{y} = [y_1 \; y_2 \; y_3]$, $\mathbf{a} = [a_0 \; a_1 \; a_2 \; a_3]$, $\mathbf{b} = [b_0 \; b_1 \; b_2 \; b_3]$ and $\boldsymbol{\lambda} = [\lambda_0 \; \lambda_1 \; \lambda_2 \; \lambda_3]$. The MIP formulation for regulation capacity can be put into a compact form:

$$\mathbb{q} = \mathbf{a}\boldsymbol{\lambda}^{\mathsf{T}} \tag{26}$$

$$\mathbb{p}_c = \mathbf{b}\boldsymbol{\lambda}^{\mathsf{T}} \tag{27}$$

$$\mathcal{A}_{\text{eq}}[\mathbf{y} \; \boldsymbol{\lambda}]^{\mathsf{T}} = \boldsymbol{\alpha}_{\text{eq}} \tag{28}$$

$$\mathcal{A}[\mathbf{y} \; \boldsymbol{\lambda}]^{\mathsf{T}} \leq \boldsymbol{\alpha} \tag{29}$$

$$\mathbf{y} \in \mathcal{B} \times \mathcal{B} \times \mathcal{B} \tag{30}$$

where $\mathcal{A}_{\text{eq}}$, $\mathcal{A}$, $\boldsymbol{\alpha}_{\text{eq}}$, $\boldsymbol{\alpha}$, $\mathbf{a}$ and $\mathbf{b}$ are matrices/vectors of appropriate dimensions constructed based on the coefficients in Equations (16)–(25). The obtained piece-wise fit for the regulation capacity shown in Figure 6 has the following parameter values: $\mathbf{a} = [0 \; 0.45 \; 0.77 \; 1]$ and $\mathbf{b} = [0 \; 0 \; 0.365 \; 0]$.
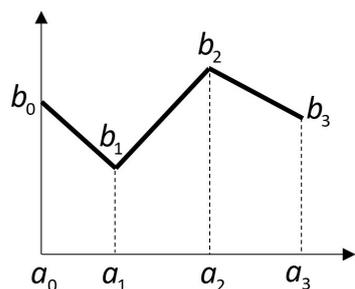

Figure 7. A general 3-segment piece-wise linear function.

The supervisory scheduling problem is then reformulated as

$$\min \sum_{i \in \mathcal{I}_k} \left\{ p[i] \cdot r_e[i] \cdot \Delta t - \mathbf{b}\boldsymbol{\lambda}^{\mathsf{T}}[i] \cdot \overline{p}[i] \cdot r_{fr}[i] \right\} \tag{31}$$

where

$$p[i] = \mathbb{p}[i] \cdot \overline{p}[i] \tag{32}$$

$$\mathbb{p}[i] = \max(0.58\mathbf{a}\boldsymbol{\lambda}^{\mathsf{T}}[i], 1.31\mathbf{a}\boldsymbol{\lambda}^{\mathsf{T}}[i] - 0.33) \tag{33}$$

subject to ($\forall i \in \mathcal{I}_k$)

$$\mathbf{x}[i+1] = \mathbf{A}\mathbf{x}[i] + \mathbf{B}_w\mathbf{w}[i] + \mathbf{B}_u\mathbf{a}\boldsymbol{\lambda}^{\mathsf{T}}[i] \cdot \overline{q}[i], \tag{34}$$

$$T_{lb}[i+1] \leq \mathbf{C}\mathbf{x}[i+1] \leq T_{ub}[i+1], \tag{35}$$

$$\mathcal{A}_{\text{eq}}[\mathbf{y}[i] \; \boldsymbol{\lambda}[i]]^{\mathsf{T}} = \boldsymbol{\alpha}_{\text{eq}} \tag{36}$$

$$\mathcal{A}[\mathbf{y}[i] \; \boldsymbol{\lambda}[i]]^{\mathsf{T}} \leq \boldsymbol{\alpha} \tag{37}$$

$$\mathbf{y}[i] \in \mathcal{B} \times \mathcal{B} \times \mathcal{B} \tag{38}$$

The formulated problem is a mixed-integer convex program and is solved using the MOSEK solver [35] in the CVX MATLAB suite [36]. In the simulation tests, a 24-h look-

ahead horizon was used with a 1-h decision step, i.e., the predictive control problem was solved at each hour and only the decision for the first time step was applied.

4.3. Baseline Control Strategies

Two baseline strategies are considered for supervisory load scheduling to assess the performance improvement of the proposed optimal control strategy. Both baseline strategies adopt the same regulation capacity reset strategy as described in Section 4.1 and they differ only in the mechanism used for determining the ZAT setpoint (sensible load).

The first baseline strategy, referred to as BaseControl I, applies conventional night setup/setback control for the ZAT with the setpoints identical to the upper/lower limits used in the optimal control. In this strategy, the minimum cooling/heating power is used to prevent the ZAT from drifting out of the comfort zone. BaseControl I can be easily implemented without any optimization procedure:

$$q_{ht}[i] = (\mathbf{CB}_u)^{-1}(T_{lb}[i+1] - \mathbf{CAx}[i] - \mathbf{CB}_w\mathbf{w}[i])$$
$$q_{cl}[i] = (\mathbf{CB}_u)^{-1}(T_{ub}[i+1] - \mathbf{CAx}[i] - \mathbf{CB}_w\mathbf{w}[i])$$
$$q[i] = \max(q_{ht}[i], 0) + \min(q_{cl}[i], 0)$$

The second baseline strategy, referred to as BaseControl II, solves the same optimal control problem in Equations (31)–(38) but with a modified objective function that includes the energy cost only:

$$\min \sum_{i \in \mathcal{I}_k} \{p[i] \cdot r_e[i] \cdot \Delta t\} \tag{39}$$

Since the MIP formulation is mainly used for predicting the piece-wise regulation capacity, which is not needed in BaseControl II, the mixed integer constraints in Equations (36)–(38) can be dropped and $\mathbf{a}\boldsymbol{\lambda}^\top$ needs to be replaced by $\mathbb{q}$ with an additional constraint of $\mathbb{q} \leq 1$. The supervisory scheduling problem for BaseControl II is convex and is solved with the SDPT3 solver [37]. The same look-ahead time horizon and decision step settings as in the optimal control strategy are used.

5. Case Study Results

All three control strategies were simulated for five summer weekdays. The ZAT lower and upper limits assume $T_{lb} = 20.5\,^\circ\text{C}$ and $T_{ub} = 24.5\,^\circ\text{C}$ during unoccupied hours and $T_{lb} = 21.5\,^\circ\text{C}$ and $T_{ub} = 23.5\,^\circ\text{C}$ for occupied periods. The building is occupied from 9 a.m. to 9 p.m. and unoccupied for the rest of the day. The simulations used actual weather and electrical load measurements taken in the case study building for a summer week as external excitation. Perfect weather and internal gain predictions were assumed in the predictive control implementations (for optimal control and BaseControl II only).

For simulation-based control performance assessment, a common practice is to use a high-fidelity plant model to emulate the detailed system behaviors while the controller employs a simpler model for ease of control implementation. In this simulation study, the envelope model trained using field measurements was employed for both the control and plant models, because the model well captures the envelope dynamics with extensive validations and is more suitable to use than a high-fidelity model without careful calibrations. For AC power calculation, the plant model assumed the original comprehensive AC model described in Equation (3) while the control model (for BaseControl II and optimal strategies only) used the piece-wise linear fit given in Equation (15). For determining regulation capacity, the plant model relied on the pseudo-optimization routine described in Equations (5)–(10) and the control model adopted the mixed-integer formulation given in Equations (26)–(30). At each hour, the optimal ZAT setpoint is determined by the supervisory scheduler, the corresponding cooling/heating load is calculated with the envelope model, and the AC power and regulation capacity are evaluated via the plant models. Table 1 summarizes the resultant energy costs and regulation credits for the various cases.

Table 1. Cost comparisons for different control scenarios.

Control Strategy	Energy Cost ($)	Reg. Credit ($)	Net Cost ($)
BaseCtrl I	0.97	0.19	0.78
BaseCtrl II	0.94 (3%↘)	0.14 (26.3%↘)	0.8 (2.5%↗)
OptimalCtrl	0.99 (2%↗)	0.32 (118.6%↗)	0.67 (14.1%↘)

Figure 8 shows the 5-day simulation results for BaseControl I. The top subplot gives the variations of the simulated ZAT as well as the upper and lower limits. The bottom subplot depicts the AC power use and the band of power modulation for frequency regulation; the latter was estimated with the regulation capacity reset controller described in Section 4.1. It can be seen that mechanical cooling is requested for a majority of the occupied hours. The first two days are relatively cool with low cooling loads. For the first day, the load is always lower than the AC minimum cooling output, leading to cyclic operations for most of the occupied period. As a consequence, there is no regulation capacity available for the first day. The second day is slightly warmer with the cooling load higher than the minimum AC cooling output in the afternoon, resulting in some regulation flexibility. For the remaining three days, the AC system can provide good amount of regulation service in the afternoon when the cooling load is moderate. During unoccupied hours, no regulation service can be provided due to the low or zero cooling demand.
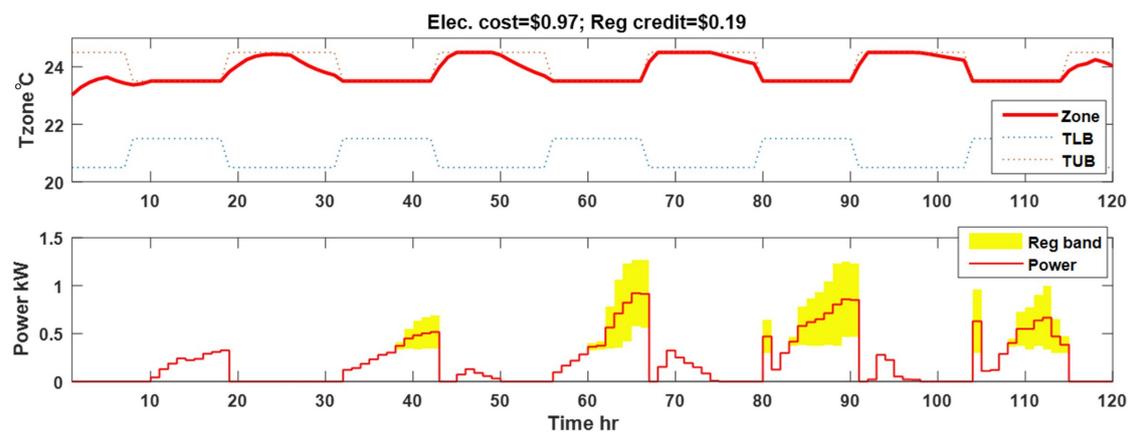

Figure 8. BaseControl I results.

Figure 9 presents the simulation results for BaseControl II. A third subplot is included that shows variations of the whole energy and frequency regulation prices. The simulations used the annual averaged prices shown in Figure 3 and assumed identical price profiles for all simulation days. Although the regulation price is not used in the BaseControl II strategy, it is included to illustrate the necessity for an improved control strategy. Compared to the BaseControl I results, a major difference in the BaseControl II simulation results is the existence of precooling and load shedding on days 3 to 5. BaseControl II tends to precool the building in early morning hours (e.g., hours 52 to 56) when the energy price is low in order to reduce the AC energy use during high-price periods. Other driving factors for building precooling include (1) shifting loads to periods having a lower ambient temperature to achieve a higher cooling efficiency and (2) flattening the load profile to leverage the higher efficiency during part-load operations. The latter can be reflected by the fact that the AC unit is operated at or below the minimum cooling capacity, when the cooling efficiency is the highest, for longer periods of time, as evidenced by the histogram plot of the load ratio (q) in Figure 10. Compared to BaseControl I, the BaseControl II strategy can reduce the energy cost by more than 3%. However, the BaseControl II leads to a regulation credit 26.3% lower than the BaseControl I case. That is because the BaseControl

II strategy operates the AC system at or below the minimum cooling output more often, resulting in a lower integrated regulation capacity.
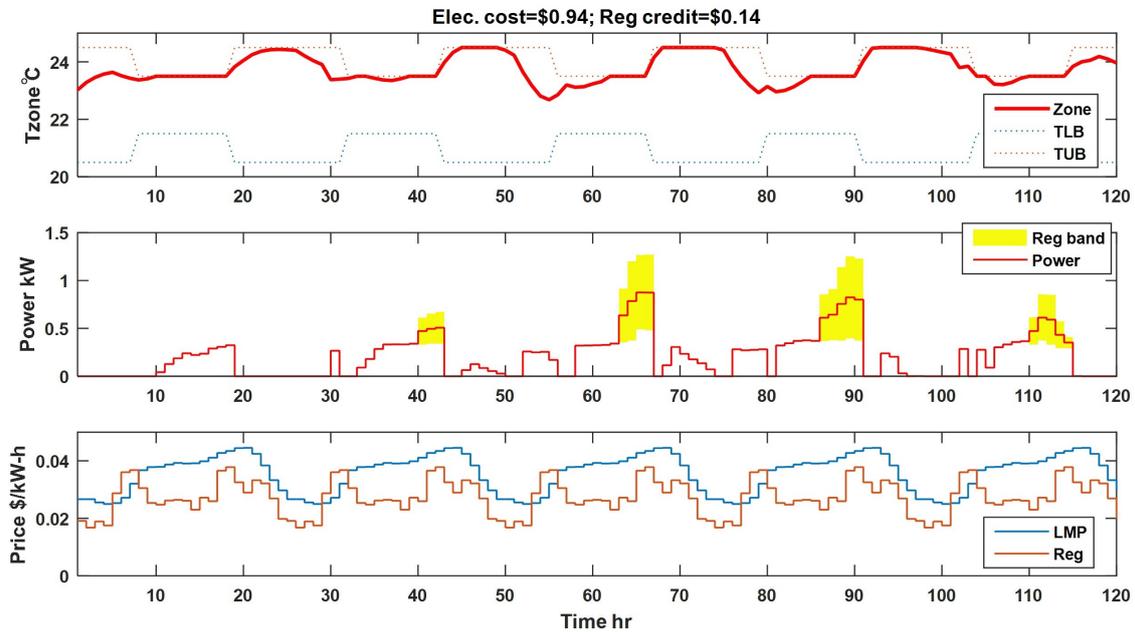

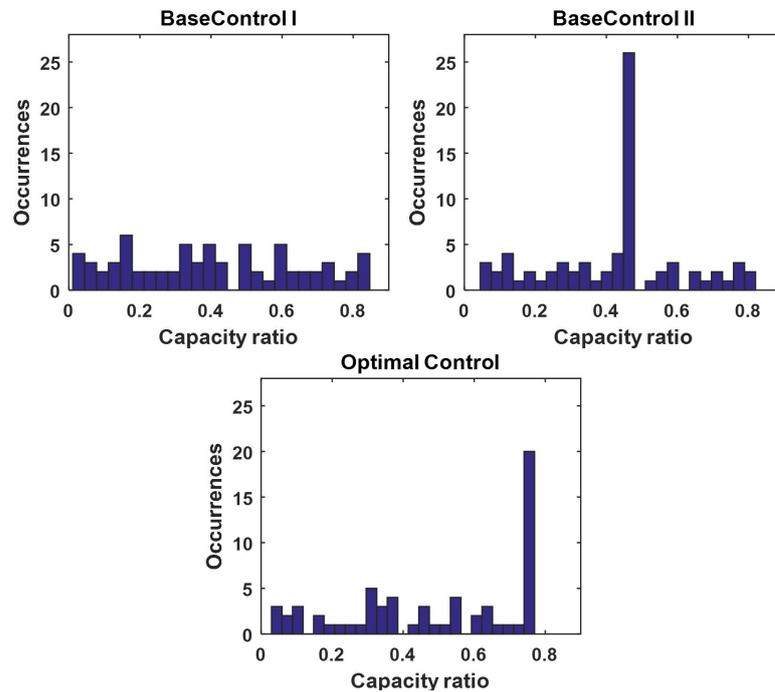**Figure 9.** BaseControl II results.

Figure 10. Histograms of the load ratio associated with the different control strategies.

The optimal control results are plotted in Figure 11. Precooling is also present in the optimal results. Compared to BaseControl II, the major difference is that the optimal control precools the building for all five days, and the precooling periods are better aligned with the high regulation price hours. In addition, the precooling power is maintained close to the middle of the power modulation range to provide the maximum regulation capacity. During regular cooling hours, the AC power is also kept at a favorable level for longer periods of time to increase the regulation availability. This pattern can also be observed in the histogram plot in Figure 10: the most frequent load ratio occurs at 0.77 when the available

regulation capacity is the highest. There is a clear trade-off in the control decision making between efficiency (energy cost) and power flexibility (regulation credit): for a lower cooling load, the energy efficiency is higher but the available regulation capacity is limited; a higher cooling demand results in a lower efficiency but leads to improved power flexibility (only up to load ratio of 0.77); excessively high cooling load is not favorable for either efficiency or regulation capacity. The optimal control strategy is able to identify the balancing point; although the energy cost of the optimal control is 2% higher than BaseControl I and 5% greater than BaseControl II, a significantly higher regulation credit can be achieved, 68.4% greater than that of BaseControl I and 118.6% higher than the BaseControl II regulation credit. The net electricity cost is reduced by 14.1% compared to BaseControl I results and by 16.3% from BaseControl II results.

Mismatch between the control model and the actual plant dynamics (plant model) could cause sub-optimality in the obtained control decisions. To evaluate the model discrepancies and the impact on the control performance, Figure 12 compares the AC power and regulation band estimated using the control and plant (simulation) models. It can be seen that the control model can predict both the AC power and regulation capacity with satisfactory accuracy. The prediction errors for the integrated energy cost and regulation credit were within 3% compared to the results obtained using the plant model.
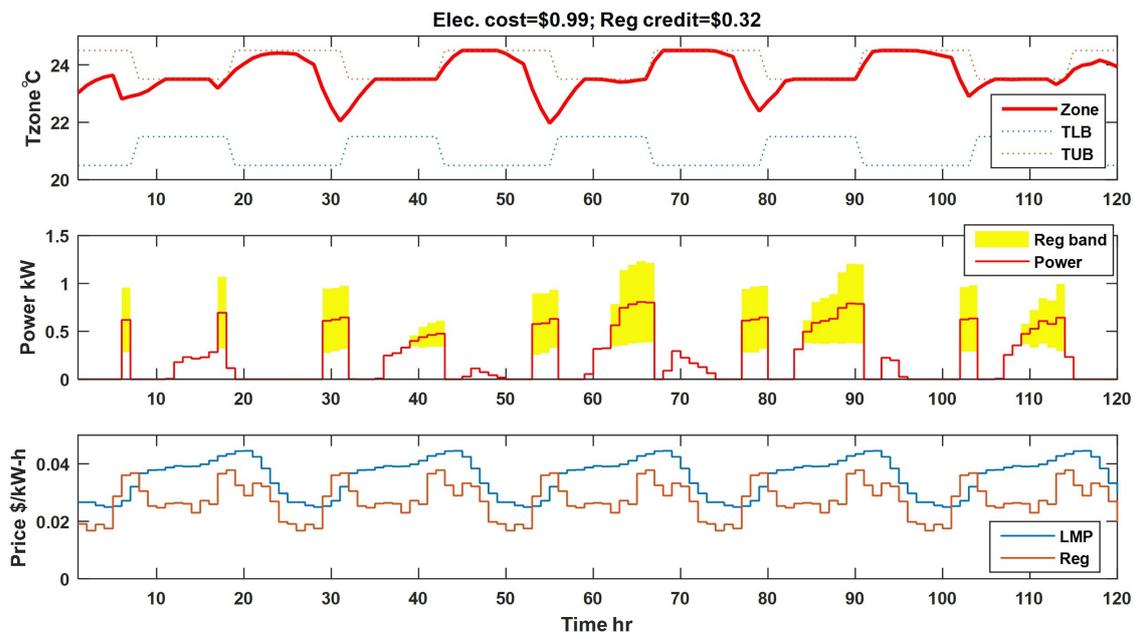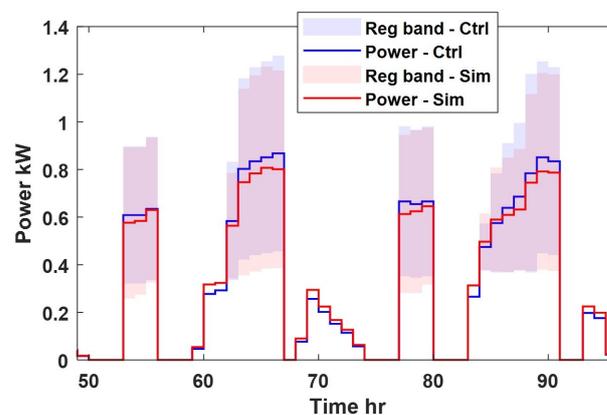

Figure 11. Optimal control results.

Figure 12. Comparison of control- and simulation-model results using the optimal control actions.

6. Conclusions

This paper presented a bi-market control solution to support a building's participation in the wholesale energy and frequency regulation markets. The control solution was built on top of a previously developed frequency regulation strategy for variable-capacity AC systems, and incorporates a predictive control strategy to identify the optimal ZAT and load schedules to achieve the minimum net operation cost. The scheduling algorithm sits on top of a regulation capacity reset strategy that is implemented every hour for maximizing the power flexibility for frequency regulation. Due to the existence of nonlinearity and mode switches in the regulation capacity reset strategy, the integrated control problem is difficult to solve directly. To improve the computational feasibility, piece-wise linear fits were obtained from an offline analysis to approximate the lower-level regulation capacity reset behaviors and a mixed-integer convex program was formulated, which can be solved efficiently using mature solvers.

To demonstrate the effectiveness of the proposed control strategy, simulation tests were carried out for an office building using historical PJM wholesale energy and regulation prices. Two baseline strategies were also simulated to evaluate the performance gains of the proposed strategy: the first baseline strategy, BaseControl I, assumes a conventional night setup/setback control for the ZAT setpoint and the other strategy, BaseControl II, relies on solving a similar optimal control problem but with an objective function including the energy cost only. Test results have shown that energy cost-priority strategies, such as BaseControl II, could lead to even higher net costs, due to the limited frequency regulation flexibility. The proposed strategy was able to find the balancing point between the energy cost and regulation credit, resulting in a minimum net cost. Compared to the conventional night setup/back strategy, the proposed control solution resulted in a net cost reduction of 14% and an integrated regulation credit increase by 118%.

Institutional Review Board Statement: Not applicable.

Informed Consent Statement: Not applicable.

Data Availability Statement: The data presented in this study are available on request from the author.

References

1. What Are the Questions Raised by the UK's Recent Blackout? Available online: https://www.theguardian.com/business/2019/aug/12/what-are-the-questions-are-raised-by-the-uks-recent-blackout (accessed on 15 September 2019).
2. Zhou, Z.; Levin, T.; Conzelmann, G. *Survey of US Ancillary Services Markets*; Technical Report; Argonne National Lab. (ANL): Argonne, IL, USA, 2016.
3. EIA, Use of Electricity Explained. Available online: https://www.eia.gov/energyexplained/index.php?page=electricity_use (accessed on 30 January 2019).
4. Lin, Y.; Barooah, P.; Meyn, S.; Middelkoop, T. Experimental evaluation of frequency regulation from commercial building HVAC systems. *IEEE Trans. Smart Grid* **2015**, *6*, 776–783. [CrossRef]
5. MacDonald, J. *Commercial Building Loads Providing Ancillary Services in PJM*; Lawrence Berkeley National Lab. (LBNL): Berkeley, CA, USA, 2014.
6. Fabietti, L.; Gorecki, T.T.; Qureshi, F.A.; Bitlislioğlu, A.; Lymperopoulos, I.; Jones, C.N. Experimental implementation of frequency regulation services using commercial buildings. *IEEE Trans. Smart Grid* **2016**, *9*, 1657–1666. [CrossRef]
7. Wang, H.; Wang, S.; Tang, R. Investigation on the Use of Pumps in HVAC Systems for Providing Ancillary Services in Smart Grids. *Energy Procedia* **2019**, *159*, 219–224. [CrossRef]
8. Kim, Y.J.; Fuentes, E.; Norford, L.K. Experimental study of grid frequency regulation ancillary service of a variable speed heat pump. *IEEE Trans. Power Syst.* **2015**, *31*, 3090–3099. [CrossRef]
9. Motalleb, M.; Thornton, M.; Reihani, E.; Ghorbani, R. Providing frequency regulation reserve services using demand response scheduling. *Energy Convers. Manag.* **2016**, *124*, 439–452. [CrossRef]
10. Su, L.; Norford, L.K. Demonstration of HVAC chiller control for power grid frequency regulation—Part 1: Controller development and experimental results. *Sci. Technol. Built Environ.* **2015**, *21*, 1134–1142. [CrossRef]

11. Cai, J.; Braun, J.E. Laboratory-based assessment of HVAC equipment for power grid frequency regulation: Methods, regulation performance, economics, indoor comfort and energy efficiency. *Energy Build.* **2019**, *185*, 148–161. [CrossRef]

12. Rotger-Griful, S.; Chatzivasileiadis, S.; Jacobsen, R.H.; Stewart, E.M.; Domingo, J.M.; Wetter, M. Hardware-in-the-loop co-simulation of distribution grid for demand response. In Proceedings of the 2016 Power Systems Computation Conference (PSCC), Genoa, Italy, 20–24 June 2016; pp. 1–7.

13. Williams, S.; Short, M.; Crosbie, T. On the use of thermal inertia in building stock to leverage decentralised demand side frequency regulation services. *Appl. Therm. Eng.* **2018**, *133*, 97–106. [CrossRef]

14. Callaway, D.S. Tapping the energy storage potential in electric loads to deliver load following and regulation, with application to wind energy. *Energy Convers. Manag.* **2009**, *50*, 1389–1400. [CrossRef]

15. Shi, Q.; Li, F.; Hu, Q.; Wang, Z. Dynamic demand control for system frequency regulation: Concept review, algorithm comparison, and future vision. *Electr. Power Syst. Res.* **2018**, *154*, 75–87. [CrossRef]

16. Beil, I.; Hiskens, I.; Backhaus, S. Round-trip efficiency of fast demand response in a large commercial air conditioner. *Energy Build.* **2015**, *97*, 47–55. [CrossRef]

17. Raman, N.S.; Barooah, P. On the round-trip efficiency of an HVAC-based virtual battery. *IEEE Trans. Smart Grid* **2019**, *11*, 403–410. [CrossRef]

18. MacDonald, J.; Cappers, P.; Callaway, D.; Kiliccote, S. Demand response providing ancillary services: A comparison of opportunities and challenges in the US wholesale markets. In Proceedings of the Grid Interop 2012, Irving, TX, USA, 3–6 December 2012.

19. Energy and Ancillary Services Market Operations. Available online: https://www.pjm.com/-/media/documents/manuals/m11.ashx?la=en (accessed on 30 January 2019).

20. Balandat, M.; Oldewurtel, F.; Chen, M.; Tomlin, C. Contract design for frequency regulation by aggregations of commercial buildings. In Proceedings of the 2014 52nd Annual Allerton Conference on Communication, Control, and Computing (Allerton), Monticello, IL, USA, 30 September–3 October 2014; pp. 38–45.

21. Vrettos, E.; Oldewurtel, F.; Andersson, G. Robust Energy-Constrained Frequency Reserves From Aggregations of Commercial Buildings. *IEEE Trans. Power Syst.* **2016**, *31*, 4272–4285. [CrossRef]

22. Iria, J.; Soares, F.; Matos, M. Optimal bidding strategy for an aggregator of prosumers in energy and secondary reserve markets. *Appl. Energy* **2019**, *238*, 1361–1372. [CrossRef]

23. Vrettos, E.; Andersson, G. Scheduling and Provision of Secondary Frequency Reserves by Aggregations of Commercial Buildings. *IEEE Trans. Sustain. Energy* **2016**, *7*, 850–864. [CrossRef]

24. Maasoumy, M.; Rosenberg, C.; Sangiovanni-Vincentelli, A.; Callaway, D.S. Model predictive control approach to online computation of demand-side flexibility of commercial buildings HVAC systems for supply following. In Proceedings of the 2014 American Control Conference, Portland, OR, USA, 4–6 June 2014; pp. 1082–1089.

25. Vrettos, E.; Kara, E.C.; MacDonald, J.; Andersson, G.; Callaway, D.S. Experimental demonstration of frequency regulation by commercial buildings—Part I: Modeling and hierarchical control design. *IEEE Trans. Smart Grid* **2016**, *9*, 3213–3223. [CrossRef]

26. Vrettos, E.; Kara, E.C.; MacDonald, J.; Andersson, G.; Callaway, D.S. Experimental demonstration of frequency regulation by commercial buildings—Part II: Results and performance evaluation. *IEEE Trans. Smart Grid* **2016**, *9*, 3224–3234. [CrossRef]

27. Blum, D.H.; Xu, N.; Norford, L.K. A novel multi-market optimization problem for commercial heating, ventilation, and air-conditioning systems providing ancillary services using multi-zone inverse comprehensive room transfer functions. *Sci. Technol. Built Environ.* **2016**, *22*, 783–797. [CrossRef]

28. Blum, D.H.; Zakula, T.; Norford, L.K. Opportunity cost quantification for ancillary services provided by heating, ventilating, and air-conditioning systems. *IEEE Trans. Smart Grid* **2016**, *8*, 1264–1273. [CrossRef]

29. Pavlak, G.S.; Henze, G.P.; Cushing, V.J. Optimizing commercial building participation in energy and ancillary service markets. *Energy Build.* **2014**, *81*, 115–126. [CrossRef]

30. Cai, J. A Low Cost Multi-Agent Control Approach for Building Energy System Management. Ph.D. Thesis, Purdue University, West Lafayette, IN, USA, 2015.

31. Cai, J.; Braun, J.E. A regulation capacity reset strategy for HVAC frequency regulation control. *Energy Build.* **2019**, *185*, 272–286. [CrossRef]

32. Cai, J.; Braun, J. An inverse hygrothermal model for multi-zone buildings. *J. Build. Perform. Simul.* **2016**, *9*, 510–528. [CrossRef]

33. Cai, J.; Braun, J.E. Assessments of variable-speed equipment for packaged rooftop units (RTUs) in the United States. *Energy Build.* **2018**, *164*, 203–218. [CrossRef]

34. PJM Operating Agreement Accounting. Available online: https://www.pjm.com/-/media/documents/manuals/m28.ashx?la=en (accessed on 30 January 2019).

35. The MOSEK Optimization Software. 2010. Available online: http://www.mosek.com (accessed on 1 March 2020).

36. Grant, M.; Boyd, S.; Ye, Y. CVX: Matlab Software for Disciplined Convex Programming. 2008. Available online: http://cvxr.com/cvx/ (accessed on 1 March 2020).

37. Toh, K.C.; Todd, M.J.; Tütüncü, R.H. SDPT3: A MATLAB software package for semidefinite programming, version 1.3. *Optim. Methods Softw.* **1999**, *11*, 545–581. [CrossRef]